Coronary Artery Numerical Flow Analysis for Determination of Bypass Graft Geometric Parameters

Hyung Min Kim*
Division of Mechanical System Design Engineering, Kyonggi University,
San 94-6, Yiui-Dong, YoungTong-Ku, Suwon-Shi, Kyonggi-Do 442-760, Korea
Woong Kim
Graduate School of Mechanical Engineering, Kyonggi University,
San 94-6, Yiui-Dong, YoungTong-Ku, Suwon-Shi, Kyonggi-Do 442-760, Korea

A computational investigation of blood flow in a coronary artery grafted by artificial bypass was performed to determine such geometric parameters as the curvature of radius, approach length, and angle of end-to-side anastomosis. Transient flow features in the host artery were computed using FVM and SIMPLE algorithms. We compared flow distributions and wall shear stresses in two simple models, planar and non-planar, and confirmed that the non-planar bypass model was more conducive to suppressing intimal hyperplasia. Our non-planar model with 60° of anastomosis and a 1.0 diameter approach length and radius of curvature predicts a relatively small, spatially-extended high-OSI (>0.01) zone, as well as an increased average wall shear stress on this zone.

Key Words : Coronary Artery, Bypass Graft, Oscillatory Shear Index, Computational Fluid Dynamics

Nomenclature ───────────

a_n, b_n : Fourier cosine and sine coefficient
D : Diameter of host artery [m]
$\vec{n}_m$: Mean shear direction vector
Q : Flow rate [m/s]
p : Pressure [Pa]
T : Period [rad]
t : Time [s]
v_i : Velocity vectors [m/s]
x_i : Coordinate [m]
α : Angle between $\vec{\tau}$ and $\vec{n}_m$
ρ : Density [kg/m²]
$\vec{\tau}$: Shear stress vector [N/m²]
τ_{wa} : Average wall shear stress [N/m²]
ν : Viscosity [m²/s]

Ω : Frequency [1/s]
w : Weighting factor

1. Introduction

Arteriosclerosis is a chronic disease in which thickening, hardening, and loss of elasticity of the arterial walls result in impaired blood circulation. Over time, arteriosclerosis causes the interior of the blood vessel to narrow and, ultimately, to stenose. For coronary arteries, this contraction is termed "critical" when the diameter of the artery has been reduced by at least 50%. Curative means are in practice, including angioplasty, stent surgery, and most recently, coronary bypass surgery. Of the many arterial bypass grafts implanted annually to relieve arterial occlusion, however, the failure rates are 25% within one year and 50% within 10 years. Failure is generally caused by stenosis secondary to intimal hyperplasia, and while the cause of the intimal hyperplasia is not fully understood, it is known that intimal hyper-

* Corresponding Author,
  E-mail : pius@kyonggi.ac.kr
  TEL : +82-31-249-9815; FAX : +82-31-249-9796
  Division of Mechanical System Design Engineering, Kyonggi University, San 94-6, Yiui-Dong, Young Tong-Ku, Suwon-Shi, Kyonggi-Do 442-760, Korea.
  (Manuscript **Received** September 20, 2004; **Revised** January 15, 2005)

plasia occurs preferentially in regions of low time-averaged shear stress and rapid temporal change in wall shear stress (Ohja et al. 1990).

The representative investigations of these phenomena are of two types: (1) correlations between intimal thickening and local flow pattern and (2) correlations between wall shear stress and bypass geometry. Recently, much research has sought to examine the correlations between local flow features, vessel wall contraction, and pathogenesis. For example, Ohja et al.(1993) found that intimal hyperplasia tends to occur in regions of low time-averaged shear stress. Asakura (1990) identified a strong correlation between regions of low wall shear and the location of atherosclerotic plaques.

Moore et al.(1999), Sherwin et al.(2000) and Papaharilaou et al.(2002) studied the associations of bypass geometry and flow. The first of these groups reported that removal of out-of-plane curvature substantially changed the secondary flow field and particle residence times, but did not markedly alter the distribution of wall shear stress. Their investigations employed a model with a hood, however, which expanded graft cross-sectional area, reduced mean velocity, and thereby lessened the effect of out-of-plane curvature on the flow field. Sherwin et al.(2000) found that a simple modification in the geometry of end-to-side anastomosis affected the flow field and influenced the particle residence times. Papaharilaou et al.(2002) also examined the influence of anastomosis geometry variations on flow patterns and wall shear stress. They concluded that all flow features, including wall shear stress and oscillatory shear index (OSI), were significantly changed by variations in geometry. Furthermore, they showed that out-of-plane curvature in the graft strongly influences perianastomotic flow and would thus be expected to affect localization of vessel wall dieses.

The present study is concerned with the influences of bypass geometry on wall shear stress in a transient pulsatile flow environment. We also discuss here several geometric parameters of the grafted bypass, including spatial bending, anastomotic angles, radius of curvature, and approach

length, so as to better characterize flow features in the coronary artery. Finally, our results may allow for clinical decisions leading to the most profitable bypass geometry by way of analyses of the velocity profile, time-averaged wall shear stress, and magnitude of OSI.

2. Numerical Technique

2.1 Numerical analysis

Numerical analysis of arterial blood flow patterns is a powerful tool for studying the relationship between hemodynamics and arterial disease pathogenesis. In this study, we focused on the variation in flow features due to changes in geometry. Consequently, Newtonian-fluid-behavior as well as rigid-wall-assumed and transient incompressible Navier-Stokes equations without body force were solved using finite volume method. The governing equations are represented by Eqs. (1) and (2).

$$\frac{\partial v_i}{\partial x_i} = 0 \qquad (1)$$

$$\left(\frac{\partial v_i}{\partial t} + v_j \frac{\partial v_i}{\partial x_j}\right) = \nu \frac{\partial^2 v_i}{\partial x_j^2} - \frac{1}{\rho}\frac{\partial p}{\partial x_i} \qquad (2)$$

Average values for blood density (1050 kg/m³) and viscosity (3.675e-3 kg/ms) were assumed in our fluid-flow models, shown in Figure 1. Representing a small artery, our host vessel had a diameter of 1.0e-3 m and length 12 times this diameter. The bypass was grafted 3.0 diameters from the occlusion end. In the planar model, the length of the graft was fixed at 5.0 diameters. For the non-planar model, the radius of curvature and approach length were variable.

The governing equations were discretized by Finite Volume Methods (FVM) in order to compute numerically the velocity fields and pressure profile. The SIMPLE (Semi-Implicit Method for Pressure-Linked Equations) algorithm was used to satisfy the continuity. We modified the research code developed by Kim (1997).

At the outflow boundary shown in Figure 1, the Neumann condition was imposed. Likewise, the no-slip condition was applied to the walls. The actual pulsatile flow rate was extracted from

a previous study by Choi et al. (1999) in which the flow was measured by clinical cardiac examination.

Figure 2 charts the physiological inlet flow rate at the coronary artery. Time points at t= 0.0 s and t=0.24 s represent the initiation of systole and diastole, respectively. The flow rate curve of the coronary artery has two maxima, 1.6e-6 m³/s and 3.5e-6 m³/s. The first peak occurs in the contraction period, the second in relaxation. The flow rate in the coronary artery never

drops below zero during a complete pulsation cycle. For an abdominal aortic aneurysm, on the other hand, the flow rate has negative magnitude during relaxation. We used the inflow boundary conditions to calculate a physiological volume flow rate. The Reynolds and Womersley numbers are 1250 and 0.3, respectively. Fourier-series expansion for the period T=0.75 s yields Eq. (3).

$$Q_{inlet} = Q_{mean} + \sum_{n=1}^{30} [a_n \cos(n\Omega t) + b_n \sin(n\Omega t)] \quad (3)$$

where $\Omega (= 2\pi/T)$ and t are the natural frequency and time, Q_{mean} is the time-averaged flow rate passing though the blood vessel, and a_n and b_n are the Fourier cosine and sine coefficients.

2.2 Shear stress and oscillatory shear index (OSI)

Following computation of the flow field, shear stress on the host artery wall could be calculated in the cylindrical coordinate system shown in Figure 3. Shear stress on the wall is defined as

$$\tau_i = \mu \left(\frac{\partial u_i}{\partial x_i} + \frac{\partial u_j}{\partial x_i} \right) \cdot n_j \quad (4)$$

Oscillatory shear index represents the oscillatory motion of the wall shear stress vector and the directional change with time in a continuous fashion. OSI was calculated by modifying the definition of Ku et al. (1985) with the formulation introduced by Moore et al. (1999).
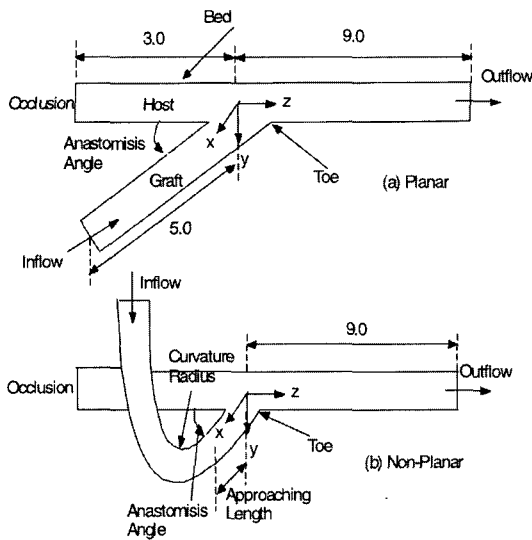

Fig. 1 Basic model geometries of planar and non -planar bypass graft

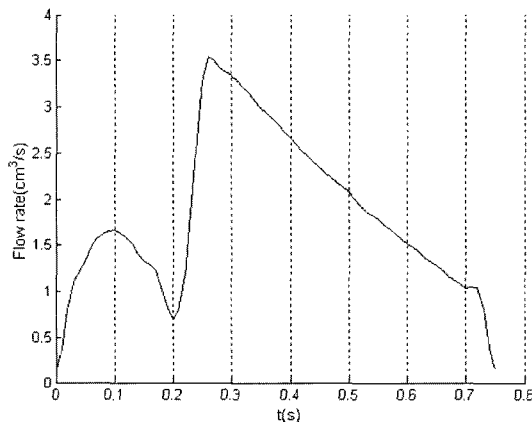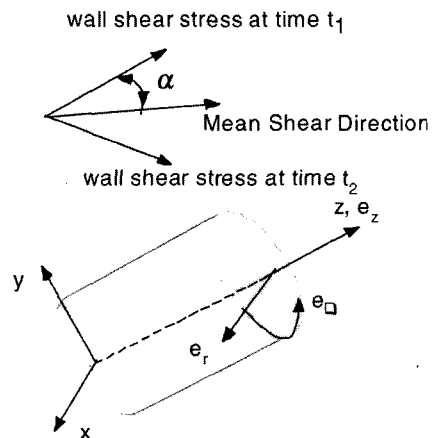**Fig. 2** Physiological flow rate at the inflow boundary (extracted from Choi (1999))

Fig. 3 Mean shear direction and the coordinate systems

$$OSI = \frac{\int_0^T w \, |\, \vec{\tau} \cdot \vec{n}_m \,|\, dt}{\int_0^T |\, \vec{\tau} \cdot \vec{n}_m \,|\, dt} \tag{4}$$

$$\vec{n}_m = \int_0^T \frac{\vec{\tau}}{|\,\vec{\tau}\,|} \, dt \tag{5}$$

where $\vec{\tau}$ is the instantaneous wall shear stress, $\vec{n}_m$ the mean shear direction, T the period of the flow waveform, and a weighting factor defined by $w = 0.5(1 - \cos \alpha)$. As shown in Figure 3, α is the angle between the initial wall shear stress and the mean shear stress vector. This definition of OSI allows for inclusion in the calculation of a continuous range of instantaneous shear vector angles with respect to the mean shear direction. The modified index ranged from 0 to 0.5, where the former corresponds to uni-directional shear flow and the latter to purely oscillatory shear.

3. Results

3.1 Comparison of planar and non-planar

Our comparison of the flow features of planar and non-planar models (shown in Figure 1) was based on the planar and non-planar models with 45° of end-to-side anastomosis considered by Papaharilaou et al.(2002). While that group employed the single harmonic sinusoidal flow waveform, however, our study saw application of the physiological flow rate inlet condition.

Figure 4 compares the spatial distribution of the axial velocity component at a secondary acc-eleration time $(t=0.25 \text{ s})$ in three locations along the host artery. One observes that the non-planar geometry breaks flow symmetry and establishes a counterclockwise bulk rotation of the z-direction velocity. Time-dependent migration in the low axial velocity region could cause the observed velocity stagnation. This rotation is evident in the host artery and is dependent on the axial downstream distance from the origin. Both models exhibit regions of flow stagnation, with their temporal and spatial evolution dependent on the downstream distance.

The computed cross-flow streamlines for two geometries are shown in Figure 5. Although it is not explicitly prescribed in the solution, flow symmetry is preserved in the planar model. Two symmetric counter-rotating vortices are also evident in the transverse plane. These vortices account, respectively, for the clockwise and counterclockwise motion of fluid particles in the upper and lower recirculation regions. The figure also illustrates breaking of the flow symmetry in the non-planar model due to an increased cross-flow magnitude as compared to the planar model. Although two counter-rotating cells can still be identified at z/D=0.5 in the non-planar plot, the lower cell is significantly stronger than the upper. As a result of the dominant counterclockwise vortex, which has its core at the bottom of the cross section, the weaker secondary clockwise vortex at the upper side of the cross section is spatially constrained. By z/D=3.0 downstream from the origin, the core of the dominant vortex
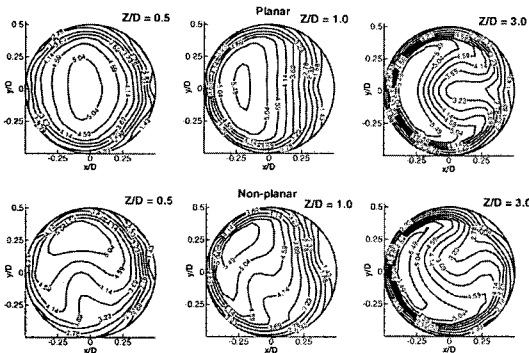

Fig. 4 Axial velocity contour plots extracted at z/D=0.5, 1.0 and 3.0
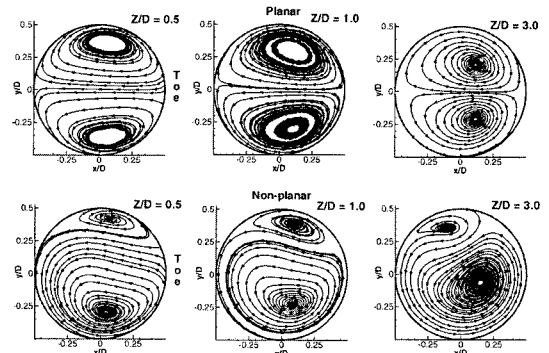

Fig. 5 Streamlines plot of the secondary flow at z/D=0.5, 1.0 and 3.0 from the origin

has rotated counterclockwise by almost 90° and the weak secondary vortex has begun to disappear.

In Figure 6, one sees a comparison of the numerically-computed wall shear streamlines and OSI distributions on the unfolded artery wall of the planar and non-planar models at the time of secondary acceleration. The points of convergence or divergence of the streamlines indicate stagnation or separation of stress. These points coincide with the shape of the OSI (>0.01) distribution and of minimal shear stress. Accordingly, we defined the lower limit of "high OSI" to be 0.01.

High OSI localizes to the bedside (opposite side of the conjunction hole) and takes the form of a symmetrical triangle with respect to the z-axis. For the non-planar model, stagnation points are found along a line oblique to the z-axis due to the bulk flow rotation. The high–OSI zone comprises a region of low time-averaged wall shear stress and has an anti-symmetric form. In our model, wall shear stress was reduced by more than 22% in the region for which the OSI was greater than 0.01.

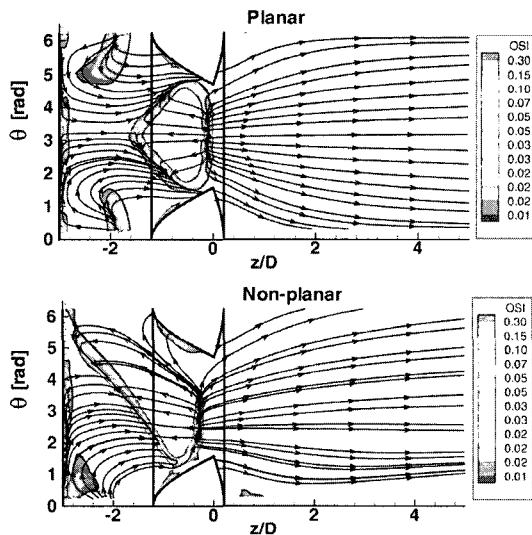Ohja et al.(1990) report that intimal hyperplasia tends to occur in these regions of low time-averaged shear stress and high OSI. Regions of OSI greater than 0.01 in our model thus represent probable localizations of vessel wall disease.

3.2 Influence of anastomotic angle

Computationally, we sought to determine the angle of anastomosis that would reduce the physical size of the high–OSI zone while simultaneously increasing the wall shear stress on the zone using end–to–side grafted non–planar bypass models with anastomotic angles of 60°, 90°, and 120°.

Figure 7 shows contour plots of OSI and wall shear stress streamlines on the unfolded artery wall the summarized results are presented in Table 1. As illustrated, the OSI distributions for the grafts with 60° and 45° of anastomosis were not significantly different, and while the high–OSI zone was larger in the 60° model than in the 45° model, the wall shear stress was also increased by more than 8% in the former. Sixty degrees of anastomosis would thus be more effective in suppressing intimal hyperplasia.
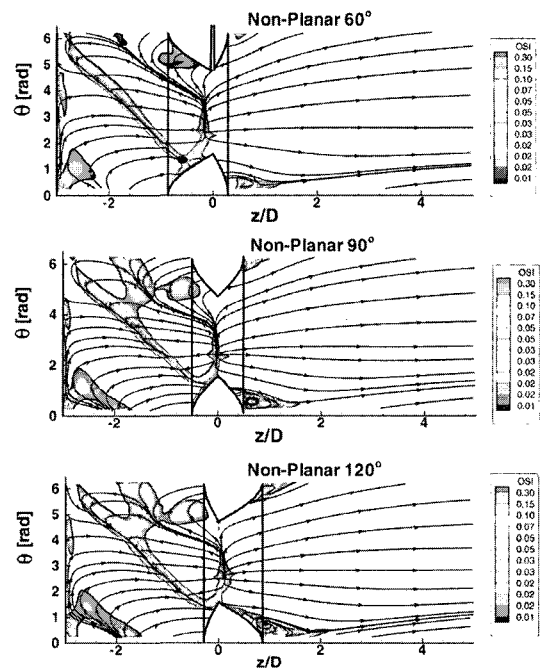

Fig. 6 Shear stress stream lines and OSI contour plots of planar and non-planar with 45° anastomotic angle

Fig. 7 Shear stress stream lines and OSI contour plots of non-planar with 60°, 90° and 120° of anastomotic angle

Table 1 Comparison of computed results for anastomotic angle variations (*denote reference)

Model	Anastomosis Angle	Area of Zone (OSI>0.01)	$\dfrac{\tau_{wa} - \tau_{wa}^*}{\tau_{wa}^*}$ (OSI>0.01)
Planar*	45°	2.430	—
Non-Planar	45°	1.973	0.55
Non-Planar	60°	2.110	0.63
Non-Planar	90°	3.114	0.92
Non-Planar	120°	3.723	1.35

Table 2 Comparison of computed results for approach length and curvature variations (* denote reference)

Approach length/D	Curvature radius/D	Area of Zone (OSI> 0.01)	$\dfrac{\tau_{wa} - \tau_{wa}^*}{\tau_{wa}^*}$ (OSI>0.01)
2.0	1.0	2.033	0.086
2.0*	2.0*	2.110	—
2.0	3.0	2.270	0.010
1.0	2.0	2.121	0.332
3.0	2.0	2.819	0.238

In the 90° and 120° models, the high–OSI zone takes the form of a "y," as seen in Figure 7. The average shear stress is increased, but its area of the high–OSI zone is increased much more. The results from all four models suggest that 60° of anastomosis in the non–planar model would give a relatively small high–OSI zone, high wall shear stress, and the greatest efficiency in suppressing the development of intimal hyperplasia.

3.3 Influence of bypass curvature and approaching length

Four new models were designed to shed light on the influences of bypass curvature radius and bypass approach length these are shown in Figure 1. Each model located the graft end–to–side with 60° of anastomosis and 1.0, 2.0, and 3.0 diameters of curvature radius and approach length. The findings from the previous section on anastomotic angle (section 3.2) allowed us to select 60° of anastomosis for these models. The boundary conditions from the previous study were applied here also.

Figure 8 shows the wall shear stress streamlines superimposed on the OSI contour plots of the unfolded artery wall for the cases of 1.0, 2.0, and 3.0 diameters of bypass curvature radius and approach length. The areas of the high–OSI zone and the rates of change of the wall shear stress (OSI >0.01) are listed in Table 2. The high–OSI distribution for 3.0 diameters of curvature radius is similar to that for the typical non–planar model. In the region near the conjunction hole, however, the area of the high–OSI zone is in-
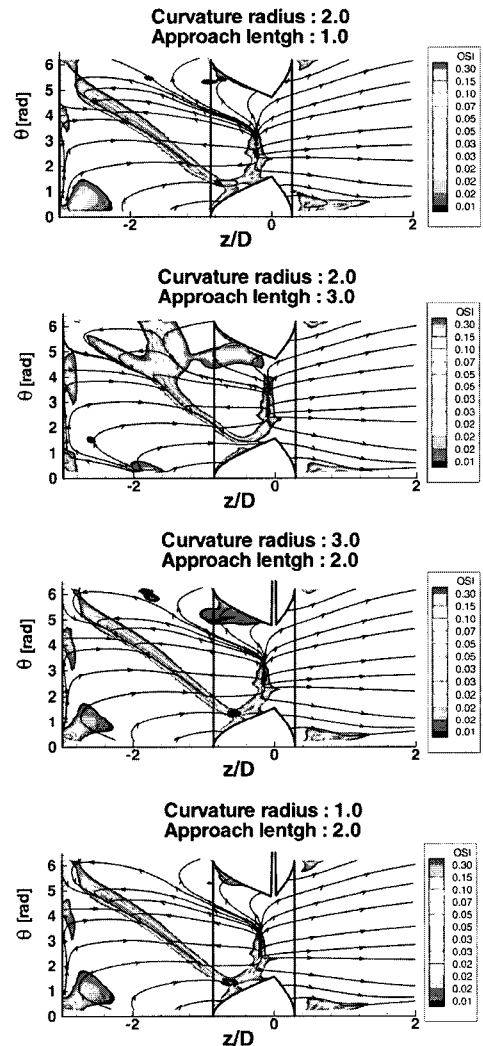

Fig. 8 Shear stress streamlines and OSI contour plots of various graft geometries with 60° of anastomosis angle

creased by 7.5% as compared to the model with 2.0 diameters of curvature radius. The area of the high-OSI zone is decreased by 3.6% for the model with a 1.0-diameter curvature radius. While wall shear stress is increased by 8.6% for the 1.0-diameter-curvature-radius model, there is no significant difference between the 2.0- and 3.0-diameter-curvature-radius models (less than 1% difference).

OSI distribution obtains a "y" shape for the model with 3.0 diameters of approach length and 90° of anastomosis (Figure 7). The area of the high-OSI zone is increased by 27.3% in this model when compared to that with 2.0 diameters of approach length. While no significant difference is seen in the area of the high-OSI zone between the 1.0- and 2.0-diameter-approach-length models, there is 30% greater shear stress in the first case. Clearly, the longer approach length leads to the weaker non-planar effect. The shorter approach length, then, would be the more effective in suppressing the development of intimal hyperplasia.

4. Conclusions

Failure of coronary bypass surgery is often attributable to stenosis secondary to intimal hyperplasia. Furthermore, intimal hyperplasia occurs preferentially in regions of low time-averaged shear stress and rapid temporal changes in wall shear stress. It may thus be possible to suppress the development of intimal hyperplasia by simultaneously reducing the area of the high-OSI zone and increasing the average wall shear stress on the host artery wall.

Area of the high-OSI zone and shear stress are closely associated with flow features in the host artery. The aim of our investigation was to demonstrate the fundamental effects of non-planar bypass geometric configurations on the flow field. As discussed previously, the flow conditions were somewhat idealized in our models. We further assumed the geometric configurations of the non-planar bypass model to be defined exclusively by anastomosis angle, curvature radius, and approach length.

While anastomotic angle did not cause major changes in flow features, we found that the shear stress on the high-OSI zone was greater by 8% in our 60° model than in our 45° model. Similarly, curvature radius did not significantly affect the magnitude of wall shear stress in the high-OSI zone. Nevertheless, the smallest high-OSI zone was formed with 1.0 diameter of curvature radius. In terms of approach length, the area of the high-OSI zone was roughly the same in the 1.0- and 2.0-diameter-approach-length models, but the magnitude of the average wall shear stress on this zone was increased by more than 30% for the shorter approach length. Although our graft models were not exhaustive of all geometries, we conclude that the non-planar bypass model with a 60° anastomotic angle, 1.0 diameter approach length, and 1.0 diameter radius of curvature would be more efficient in suppressing the development of intimal hyperplasia.

Gross geometric features are generally considered the most influential factors in vascular hemodynamics. All results in this study were based on theories of dynamics and subsequent numerical computations. We did not consider physiological complications of surgery. It would be of significant interest to extend this investigation such that bypass geometry and flow features were analyzed under real conditions.

References

Asakura, T. and Karino, T., 1990., "Flow Patterns and Spatial Distribution of Atherosclerotic Lesions in Human Coronary Arteries," *Circulation Reasearch*, Vol. 66, pp. 1045~1066

Choi Ju Hwan, Chong Sun Lee and Charn Jung Kim, 1999, "Wall Shear Stress Between Compliant Plates Under Oscillatory Flow Conditions : Influence of wall Motion, Impedance Phase Angle and Non-Newtonian Fluid," *KSME*, Vol. 25, pp. 18~28.

Kim, H. M. and Hwang, C. C., 1997, "A Turbulent Buoyant Jet in a Cross Flow," ASME-FEDSM.

Ku, D. N., Giddens, D. P., Zarins, C. K. and Glagov, S., 1985, "Pulsatile Flow and Atheros-

clerosis in the Human Carotid Bifurcation," *Arteriosclerosis*, Vol. 5, pp. 293~302.

Moore, J. A., Steinman, D. A., Prakash, S., Johnston, K. W. and Ethier, C. R., 1999, "A Numerical Study of Blood Flow Patterns in Anatomically Realistic and Simplified End-to-Side Anastomoses," *J. of Biomechanical Engineering*, Vol. 121, pp. 265~272.

Ohja, M., 1993, "Spatial and Temporal Variations of wall Shear Stress Within an End-to-Side Arterial Anastomosis Model," *J. of Biomechanics*, Vol. 26, pp. 1377~1388.

Papaharilaou, Y., Doorly, D. J. and Sherwin, S. J., 2002, "The Influence of Out-of-Plane Geromery on Pulsatile Flow Eithin a Distal End-to-Side Anastomosis," *J. of Biomechanics*, Vol. 35, pp. 1225~1239.

Sherwin, S., Shah, O., Doorly, D. J., Peiro, J., Papaharilaou, Y., Watkins, N., Caro, C. G., Dumoulin, C. L., 2000, "The Influence of Out-of-Plane Geometry on the Flow Within a Distal End-to-Side Anastomosis," *J. of Biomechanical Engineering*, Vol. 122, pp. 86~95.